*Iraqi Journal of Physics, 2025*
*https://doi.org/10.30723/ijp.v23i3.1354*

*Vol.23, No.3, PP.95-103*
*P-ISSN: 2070-4003*
*E-ISSN: 2664-5548*

# Wide Band Photoconductive Detector Based on Carbon Nanotubes Decorated with Silver Nanoparticles

**Taqwa Y. Yousif [1*], Shahd Imad Hasan[1], Asama N. Naje[2], and Estabraq A. Abed[1]**
[1]*Renewable Energy Department, College of Energy and Environmental Sciences, Al- Karkh University of Science, Baghdad, Iraq*
[2]*Department of Physics, College of Science for Women, University of Baghdad, Baghdad, Iraq*
[*]Corresponding author: taqwa.yaareb@kus.edu.iq

## Abstract
This article outlines the methodical process of manufacturing MWCNTs/SWCNTs-Ag and analyzing wideband photodetectors using a combination of electro-explosion techniques, direct mixing, and drop casting techniques. The microstructural, optical, electrical, and photo-responsive analyses of the fabricated layers were thoroughly investigated. The topographical study specifically showed that the diameter ranges from 58 to 82 nm for Ag-NPs. However, the optical spectra of the prominent layers revealed a broad absorption phenomenon along the 200–800 nm scanning wavelength. Simultaneously, the devices fabricated from SWCNTs/MWCNTs-Ag showed significant figures of merit as a function of wavelength and illumination power (365, 460, and 808 nm) in response to the applied bias voltage from 0 to 10 V. In detail, the values attained were 0.575 and 0.06 (A/W) under the 808 nm illumination wavelength for MWCNTs-Ag and SWCNTs-Ag, respectively. The figures of merit characteristics of the fabricated devices were found to be in positive linear correlation as a function of the applied wavelength.

**Article Info.**

**Keywords:**
*Photodetector, SWCNT; MWCNT, Wide Band, Responsivity.*

**Article history:**
*Received:Aug. 05, 2024*
*Revised: Dec. 25, 2025*
*Accepted:Jan. 27, 2025*
*Published:Sep. 01,2025*

## 1. Introduction
To this day, a great research effort has been demonstrated for optoelectronics application-based nanostructured semiconductor materials. This is mainly due to the active role of the nanostructured materials through which the intended application's performance could be effectively enhanced [1-3]. Within this framework, wideband optoelectronics, photodetectors in particular, are being widely considered within the research society because of their wide-reaching applications in electrical injection lasers, space-based expansion, environmental research, chemical and/or biological analysis, and optical communications [4, 5]. Detection methods can be divided into two categories based on incident photons: photovoltaic and photoconductive. The different types of photodetectors mainly include metal-semiconductor-metal, P-N junction, and metal-semiconductor with Schottky contact [6-8]. Several nanostructured semiconductor materials are being proposed to develop the addressed geometries, such as cadmium telluride (CdTe) [9], cadmium oxide (CdO) [10], and cadmium sulfide (CdS) [11] in the visible region as well as nickel oxide (NiO) [12], titanium dioxide ($TiO_2$) [13], and zinc oxide (ZnO) in the ultraviolet region [14]. Multi-walled carbon nanotubes (MWCNTs) and/or single-walled carbon nanotubes (SWCNTs) demonstrated an apprehended performance along a wide absorption range of the incident light; the addressed materials exhibited well-oriented applications in optoelectronic devices because of their excellent conductivity, flexibility, durability, etc. [15, 16]. Moreover, nanostructures-based MWCNT/SWCNT also attracted great research deal with which wide-spectrum performance is needed; for instance, $MoS_2$/CNTs and ZnO/CNTs heterostructures exhibited considerable photoresponsive rate along UV-Vis-NIR range [17-19].

The proposed study aims to study wideband photodetector-based Ag decorated with MWCNTs/SWCNTs using Si wafer in a heterojunction framework. Additionally, the microstructural and optical analysis of the deposited Ag decorated with MWCNT/SWCNT layer/s are thoroughly investigated along with the anticipated device figure of merits evaluation.

## 2. Experimental work

The electro-explosion of wire technique was utilized to prepare Ag nanostructure in distilled water; this was accomplished using a 36 V DC power supply [20]. A current of 100 A was passed to the ohmic contact through a wire connected to the negative potential. The resultant solution that contains plasma-based Ag particles was mechanically mixed with 2mL of the CNTs solutions (SWCNTs and MWCNTs, 95% Amorphous-Inc.) individually. The utilized CNTs purchased were 10-30 and 1-2 nm in diameter and 1-2 and 30 µm in length for SWCNT and MWCNT, respectively. The attained SWCNTs/MWCNTs-Ag solution was later drop cast on the Si wafer. In conjunction, finger-shaped aluminum (Al) contact was fabricated on the top of the deposited layer/s (SWCNT/MWCNT-Ag) using a thermal evaporation approach. The fabricated device along the deposited Al and the measurement set-up is elucidated in Fig. 1.

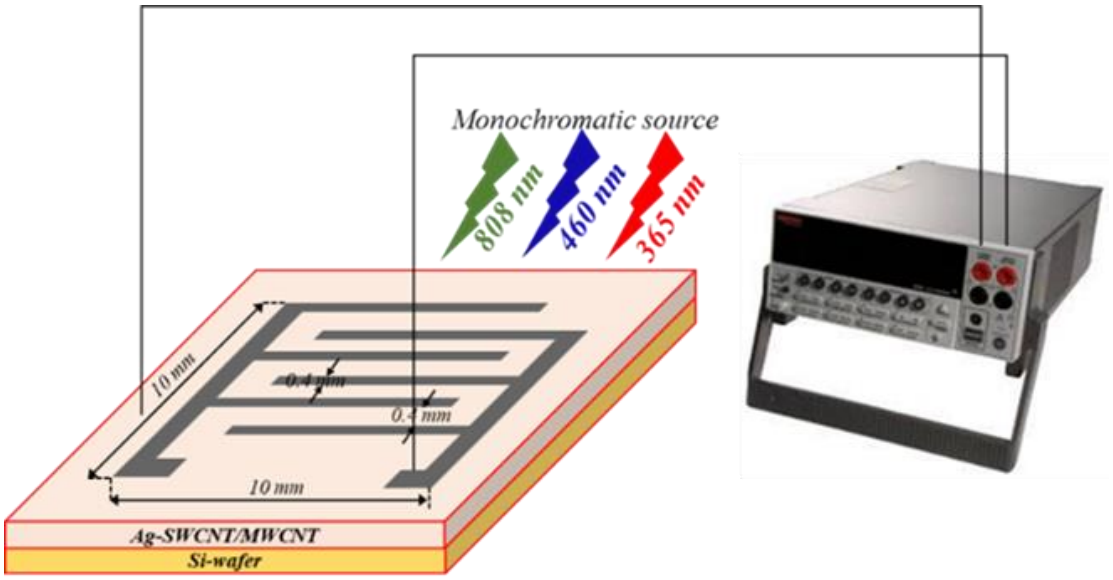


***Figure 1: Schematic representation of the measurement set-up.***

The microstructural analysis of the deposited Ag and MWCNT/SWCNT was carried out using X-ray diffractometer (HAOYUAN, XRD) and field emission scanning electron microscope (FE-SEM, MIRA3 TESCAN). The optical features were investigated using ultraviolet visible light spectroscope (UV-Vis, Shimadzu-1800). Also, Hall Effect (HMS-3000 Ecopia) technique was utilized to evaluate the deposited layer/s electrical characteristics. Herein, the fabricated photodetectors, with SWCNTs-Ag and MWCNTs-Ag layers, were analyzed in terms of current-voltage (I-V) characteristics in conjunction with a Source Measure Unit (SMU) (Keithly, 2041) under dark and multi-wavelengths monochromatic spectra (365, 460, 808 nm) emitted from a laser diode with light intensity of 6 $mW/cm^2$ focused over a 1 $cm^2$ light spot, the utilized intensity was measured using optical power density meter (Thorlabs).

## 3. Results and discussion

The XRD patterns of the prepared Ag nanoparticles, the deposited MWCNTs and SWCNTs are demonstrated in Fig. 2 (a, b, and c), respectively. The face center cubic of the prepared Ag metallic nanoparticles (Fig. 2a) was perceived at 2θ ≈ 38.1°, 44.3°, 64.6° and 77.5° regarded to the plans of (111), (200), (220), and (311), respectively; these are typically indexed to JCPDS (no. 04-0783). Fig. 2b revealed two foremost peaks attained at 2θ ≈ 26.2° (002) and 44.2° corresponded to the formation of MWCNTs (100) and (200) planes. The first peak is indexed to MWCNTs, while the second peak corresponds to the Ag metallic particles. Finally, the diffraction patterns of the fabricated SWNTs layer (Fig. 2c) demonstrated 2θ ≈ 26.2° indicating SWCNTs formation.

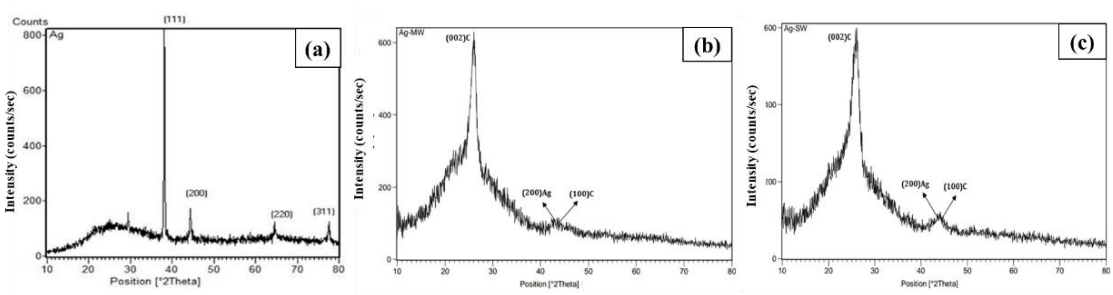


***Figure 2: XRD patterns of the fabricated layers (Ag, MWCNTs, and SWCNTs).***

The average crystallite size, as shown in Table 1, were calculated using the Debye-Scherer formula

$$D = \frac{0.9\lambda}{\beta \cos\theta_B} \qquad (1)$$

where λ is the wavelength of the X-ray source (X-ray source is Cu Kα with λ=1.5406 Å), β is the Full Width at Half Maximum (FWHM) in rad, and θ is the diffraction angle. Additionally, the dislocation density was determined according to: $\delta=1/D^2$ [21].

***Table 1: XRD parameters of Ag NPs, SWCNTs-Ag NPs and MWCNTs-Ag NPs***

| Sample | Avg. crystallite size (D) nm | dislocation density(δ) $nm^{-2}$ |
|---|---|---|
| Ag NPs | 0.58 | 2.97 |
| SWCNTs-Ag NPs | 0.88 | 1.29 |
| MWCNTs-Ag NPs | 0.91 | 1.20 |

The optical characteristics of the prepared Ag nanoparticles along the deposited MWCNTs-Ag and SWCNTs-Ag layers are elucidated in Fig. 3. The prepared Ag nanoparticles exhibited a maximum peak, so-called surface plasmon resonance (SPR), nearly around 415 nm which corresponded well to the reported data [22]. Continuously, the deposited MWCNTs-Ag and SWCNTs-Ag layers demonstrated a weak peak for the absorption phenomenon along the scanned wavelength at around 300-800 nm. The attained peaks at around 402 and 465nm mainly attributed to the surface plasmon resonance effect within silver nanoparticles [23].

The photoluminescence (PL) spectra of MWCNTs-Ag and SWCNTs-Ag at an excitation wavelength of 320nm are shown in Fig. 4. It can be observed that the MWCNTs-Ag emit peaks at 356, 459 and 536 nm with an average energy band gap of 2.8 eV. Additionally, for SWCNTs-Ag, the peaks are at 336.9, 402.5, 470, 510 and 564 nm with the average band gap energy 2.7eV. The PL spectra of MWCNTs-Ag and

SWCNTs-Ag displayed multi-luminescence peaks; the first peak is due to the intrinsic band-to-band transition, and it originated from the recombination of the free excitons. The other peaks are due to defect or impurity transition (donor-acceptor pair emission) [24].

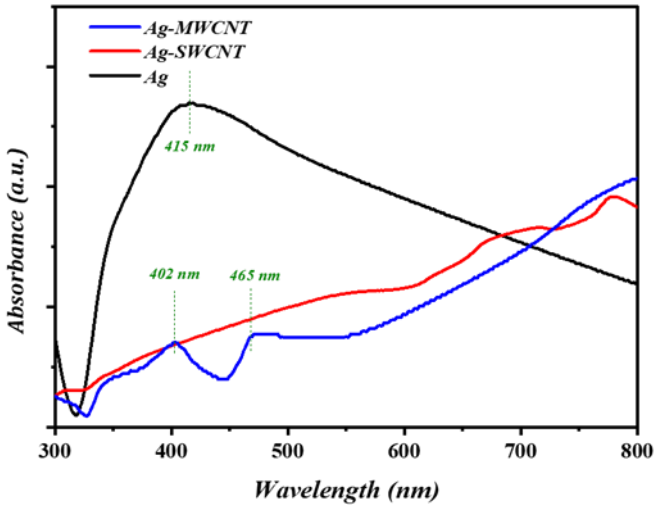


***Figure 3: Optical characteristics of Ag nanoparticles and CNTs layers.***

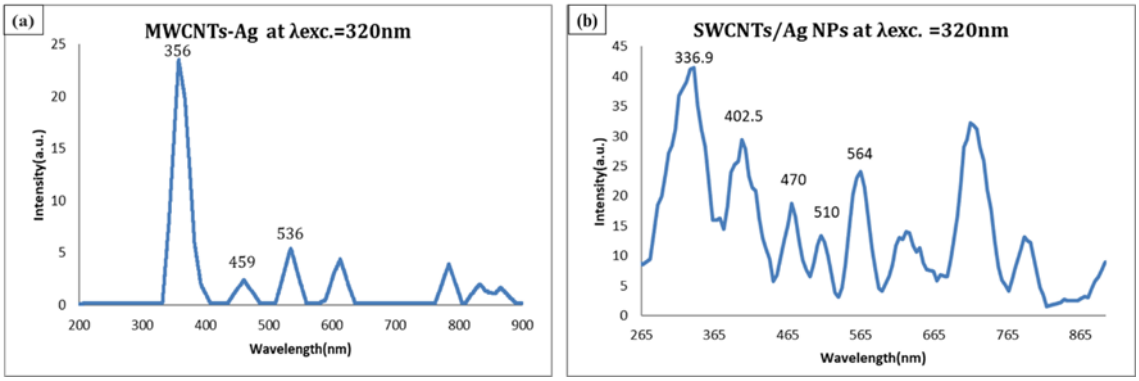


***Figure 4: The photoluminescence spectra of (a) MWCNTs-Ag (b) SWCNTs-Ag.***

Fig. 5 presents the FESEM images of Ag nanoparticles topographies with two magnifications (500 nm and 1 µm). The prepared Ag nanoparticles exhibited agglomerated nanoparticles with diameters ranging from 58 to 82 nm with a mean diameter of 70.1 nm.

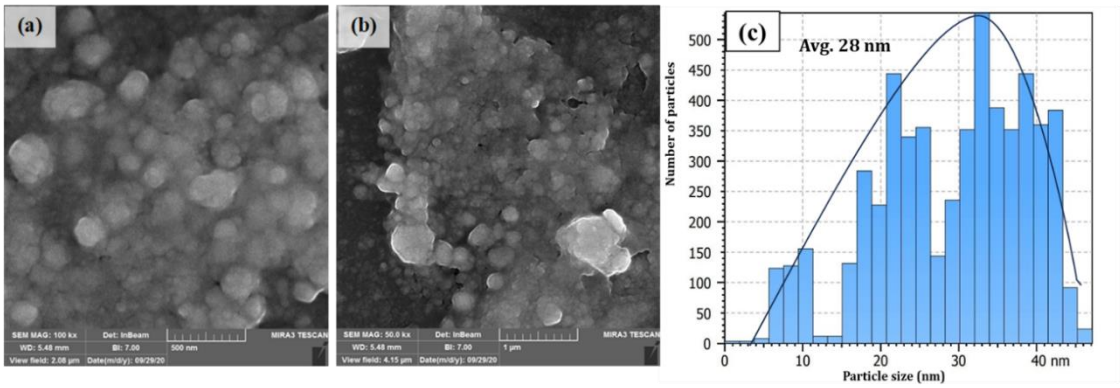


***Figure 5: FE-SEM of the prepared Ag nanoparticles, at magnifications of (a) 500 nm and (b) 1 µm (c) particle size distribution Histogram.***

Fig. 6 (a-d) shows the deposited MWCNTs-Ag and SWCNTs-Ag nanostructured layers on Si substrate with different magnifications. Both deposited layers (MWCNTs-Ag and SWCNTs-Ag) demonstrated compact and well-distributed nanostructured over the scale bar (500 nm and 1 µm). Furthermore, Ag NPs showed a reasonably uniform distribution along MWCNTs and SWCNTs surfaces. Light spots appeared on the surface of CNTs (Fig. 6 (a-d)), which indicate the silver nanoparticles. In detail, the layer attained using MWCNTs-Ag demonstrated tube diameter within the range of 39 and 52 nm with an average diameter value of 47.3 nm. Meanwhile, the SWCNTs-Ag layer demonstrated a range of diameter between 32 and 93 nm with an average of 34.6 nm.

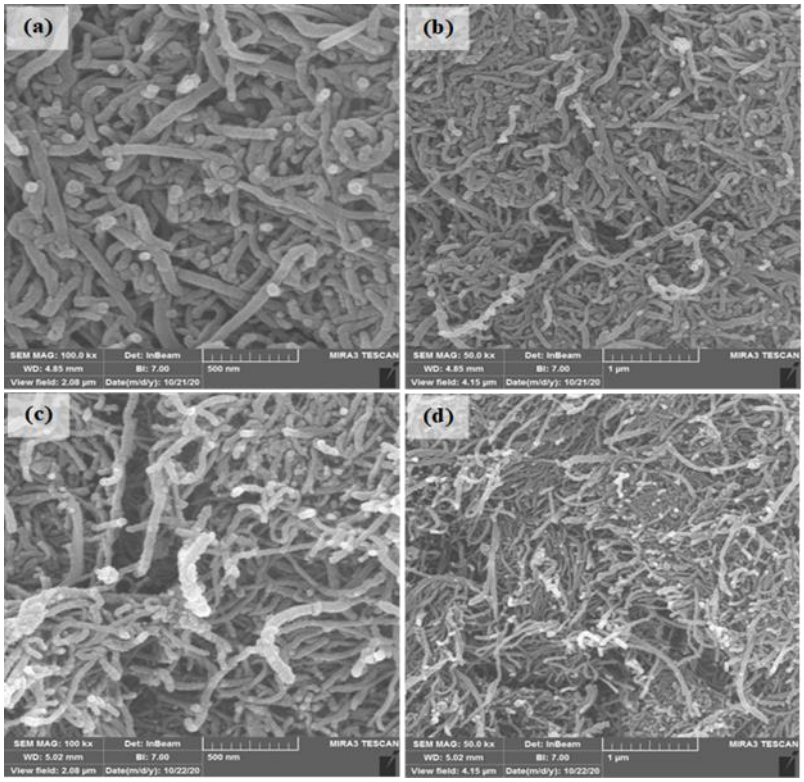


***Figure 6: FE-SEM topographies of the deposited (a) and (b) MWCNTs-Ag and (c) and (d) SWCNTs-Ag; scale bar of 500 nm and 1 µm, respectively.***

Table 2 presents the observed Hall effect parameters of the manufactured layers. It is evident from the data that MWCNTs achieved higher electrical parameters than SWCNTs.

***Table 2: Hall Measurement parameter.***

| Parameter | Charge Concentration ($1/cm^3$) | Conductivity (1/ Ω.cm) | Mobility ($cm^2/Vs$) | Resistivity (Ω.cm) | Type | Ref. |
|---|---|---|---|---|---|---|
| SWCNTs/Si | $3.1 \times 10^{17}$ | - | 62 | - | P-type | [25] |
| MWCNTs/Si | $9.516 \times 10^{18}$ | 6.25 | 3.935 | 0.16 | P-type | [26] |
| SWCNTs/Ag NPs/Si | $9.33 \times 10^{15}$ | 1.52 | $1.02 \times 10^{3}$ | 0.657 | P-type | This work |
| MWCNTs/Ag NPs/Si | $9.85 \times 10^{16}$ | 9.91 | $6.28 \times 10^{2}$ | 0.1 | P-type | This work |

The current-voltage performance of the intended devices (both MWCNTs-Ag/Si and SWCNTs-Ag/Si) is represented in Fig. 7 (a and b), respectively. In response to the sweep voltage from 0 to 10 V, the fabricated photodetectors responded exponentially as

a function of the attained current under dark and illuminated 365, 460, and 808 nm conditions. The fabricated photodetectors demonstrated a pronounced current increment upon illumination with respect to the utilized wavelength. In conjunction, both devices showed higher response under the illumination of 808 nm (IR region), which could be due to the window effect of the utilized Si wafer [10]; this behavior was not perceived for the region within UV and visible spectra. Such a singularity could be due to the fact that the utilized materials altered the optical band gaps. Furthermore, the S-shape behavior attained under the illumination of 808 nm for the MWCNTs-Ag device (Fig. 7a) could be due to an operation issue with charge carrier transport within the deposited layers; this, in turn, could be attributed to possible mismatched levels of energy and/or un-uniformed energy barrier formation at the addressed bias voltages [27].

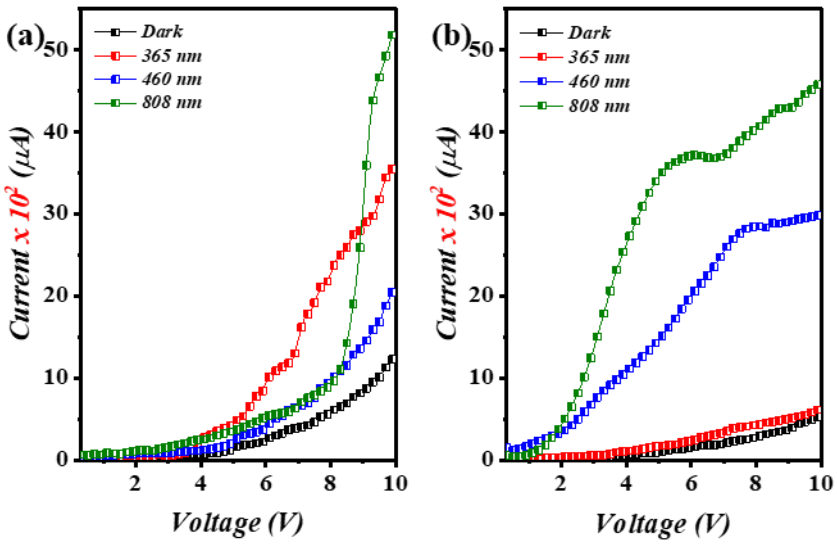


***Figure 7: Current-voltage curves of (a) MWCNTs-Ag/Si and (b) SWCNTs-Ag/Si.***

The figure-of-merits of the fabricated devices (MWCNTs-Ag/Si and SWCNTs-Ag/Si) are illustrated in Fig. 8 (a and b), respectively. The addressed parameters were using Eqs. 2-4 were used to calculate: the photocurrent ($I_{photo}$) from photoresponsivity ($R_\lambda$), photo-detectivity ($D^*$), external quantum efficiency (EQE), and photo-to-dark current ratio ($I_{photo}/I_D \times 100\%$), respectively [28-30]

$$R_\lambda = \frac{I_{photo}}{P_{in}} \tag{2}$$

$$D^* = \frac{R_\lambda A^{\frac{1}{2}}}{(2eI_D)^{\frac{1}{2}}} \tag{3}$$

$$EQE = \left[\frac{\frac{I_{photo}}{e}}{\frac{P_{in}}{hv}}\right] \tag{4}$$

where $I_D$, $P_{in}$, A, h and $v$ are the dark current, incident radiation power, the effective area of the surface, Plank constant and frequency, respectively. In general observation, the device fabricated using MWCNTs exhibited higher figure-of-merits under the illumination of 365 nm than that attained under both 460 and 808 nm, which indicates the active role of the fabricated device under UV region (Fig. 8a). Such behavior was not

found using SWCNTs, for which higher performance was found under the illumination of 808 nm (IR region). This could be explained through the optical behavior acquired during the optical properties analysis (Fig. 3). The fabricated photodetectors exhibited a considerably high rejection ratio ($I_{photo}/I_D$) with values exceeding 1000% for SWCNTs-Ag. Notably, the photodetector fabricated using SWCNTs demonstrated higher figure-of-merits than that fabricated using MWCNTs. Under 808 nm illumination, the attained $R_\lambda$ was found to be 0.575 and 0.06 (A/W) for the stated devices, respectively.

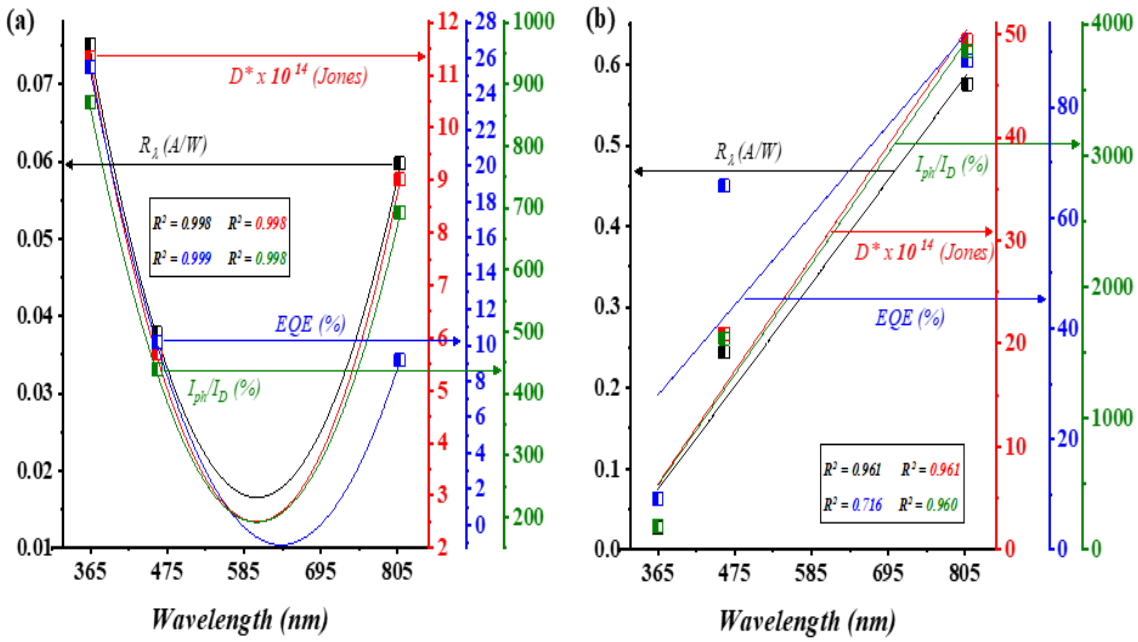


***Figure 8: Figure-of-merits for (a) MWCNTs-Ag/Si and (b) SWCNTs-Ag/Si.***

Several publications illustrating the value of using CNTs in photodetectors applications were found in the literature. The most recent publications are contrasted with the ongoing work in the following table.

***Table 3: An analysis of the suggested geometry in relation to previous published works.***

| Sample | Applied Wavelength (nm) | Responsivity (A/W) | Detectivity (Jones) | EQE (%) | Ref. |
|---|---|---|---|---|---|
| CNT/Si | 450–2400 | 0.37 | - | 50 | [16][31] |
| SWCNT/Si | 450- 2400 | - | - | 65 | [31] |
| CNT/Si | 650-1610 | 1.48 | $3.9\times10^{7}$ | - | [32] |
| MWCNT/Si | 520 -1060 | 0.72 | $1.2\times10^{10}$ | $8.77\times10^{3}$ | [33] |
| SWCNT-Ag/Si | 365-808 | 0.55 | $4.9\times10^{15}$ | 88 | This work |
| MWCNT-Ag/Si | 365-808 | 0.06 | $9.1\times10^{15}$ | 9 | This work |

## 4. Conclusions

Wide range SWCNTs-Ag and MWCNTs-Ag photodetectors of spectral response were effectively fabricated on Si substrate. The surface morphology investigation revealed the occurrence of Ag NPs with diameters ranging from 58 to 82 nm and has a reasonably uniform distribution on the surfaces of MWCNTs and SWCNTs. While, the optical analysis showed a broad range of absorption within the scanned spectrum. In conjunction, the devices that were produced with MWCNTs-Ag showed significant photo responsive characteristics and higher figure of merits when illuminated at 365 nm (UV region) in comparison to SWCNTs-Ag, which did not exhibit such a tendency, and they

performed better when illuminated in the 808 nm (IR region). Specifically, under 808 nm illumination wavelength, the obtained $R_\lambda$ for MWCNTs-Ag and SWCNTs-Ag was determined to be 0.575 and 0.06 (A/W), respectively.

## Acknowledgements

The authors would like to thank the Department of Physics, College of Science, University of Baghdad, for supporting this work.

## Conflict of Interest

The authors declare that they have no conflict of interest.

## References

1. J. Pitroda, B. Jethwa, S.K. Dave. International Journal of Constructive Research in Civil Engineering **2**, 36 (2016). https://doi.org/10.20431/2454-8693.0205007.
2. H. Chen, N. Xi, K.W. C. Lai, C. K. M. Fung, and R. Yang. IEEE Transactions on Nanotechnology, **9**, 582 (2010). https://doi.org/10.1109/TNANO.2010.2053216.
3. D. S. Ahmed, M. R. Mohammed and M. K.A. Mohammed. Nanoscience & Nanotechnology-Asia. **10**, 127 (2020). https://doi.org/10.2174/2210681208666181005145644.
4. A. S. Lanje, S. J. Sharma and R. B. Pode. Scholars Research Library Archives of Physics Research, **1**, 49 (2010).
5. D. N. Travessaa, F. S. da Silvab, F. H. Cristovana, A. M. Jorge Jr.c, K. R. Cardosoa. Materials research, **17**, 687 (2014). https://doi.org/10.1590/S1516-14392014005000026.
6. T. Y. Yousif, A. N. Naje. Journal of Physics: Conference Series, IOP Publishing, **1879**, 032093 (2021). https://doi.org/10.1088/1742-6596/1879/3/032093.
7. X. He, F. Léonard, and J. Kono, Advanced Optical Materials. **3**, 989 (2015). https://doi.org/10.1002/adom.201500237.
8. L. Liu, Y. Zhang. Sensor and Actuators A. 116, 394-397 (2004).
9. T. Ma, N. Xue, A. Muhammad, G. Fang, J. Yan, R. Chen, J. Sun, X. Sun. Micromachines. **15**, 1249 (2024). https://doi.org/10.3390/mi15101249.
10. Asama N.Naje, Ola A. Noori. International Journal of Application or Innovation in Engineering & Management (IJAIEM), **4**, 105 (2015).
11. S. Kunwar, S. Pandit, J.-H. Jeong, J. Lee. Nano-Micro Lett. **12**, (2020). https://doi.org/10.1007/s40820-020-00437-x.
12. E. Y. Salih, M. B. A. Bashir, A. H. Rajpar, I. A. Badruddin, and G. Bahmanrokh, Microelect. Eng. **258**, 111758 (2022). https://doi.org/10.1016/j.mee.2022.111758.
13. F. Salleh, R. Usop, N. S. Saugi, E. Y. Salih, M. Mohamad, H. Ikeda, M. F. Mohd Sabri, M. K. Ahmad, and S. M. Said, Appl. Surf. Sci. **497**, 143736 (2019). https://doi.org/10.1016/j.apsusc.2019.143736
14. E. Y. Salih, A. Ramizy, O. Aldaghri, M. F. Sabri, N. Madkhali, T. Alinad, K. H. Ibnaouf, and M. H. Eisa, Nanomaterials **12**, 1477 (2022). https://doi.org/10.3390/nano12091477.
15. V. S. Manikandan, S. Athithya, S. Harish, J. Archana, and M. Navaneethan, Opt. Mat. **134**, 113086 (2022). https://doi.org/10.1016/j.optmat.2022.113086.
16. A. Pelella, D. Capista, M. Passacantando, E. Faella, A. Grillo, F. Giubileo, N. Martucciello, and A. Di Bartolomeo, Adv. Elect. Mat. **9**, 2200919 (2023). https://doi.org/10.1002/aelm.202200919.
17. C. Archana, S. Harish, R. Abinaya, J. Archana, and M. Navaneethan, Sens. Actuat. A Phys. **348**, 113938 (2022). https://doi.org/10.1016/j.sna.2022.113938.
18. X. Chen, D. Bagnall, and N. Nasiri, ACS Appl. Mat. Interf. **16**, 27614 (2024). https://doi.org/10.1021/acsami.4c02284.
19. Y.-H. Lin, P.-S. Lee, Y.-C. Hsueh, K.-Y. Pan, C.-C. Kei, M.-H. Chan, J.-M. Wu, T.-P. Perng, and H. C. Shih, J. Electrochem. Soc. **158**, K24 (2011). https://doi.org/10.1149/1.3522764.
20. P. Sen, J. Ghosh, A. Abdullah, P. Kumar, and Vandana, J. Chem. Sci. **115**, 499 (2003). https://doi.org/10.1007/BF02708241.
21. I. W. Sutapa, A. W. Wahab, P. Taba, and N. L. Nafie, J. Phys. Conf. Ser. **979**, 012021 (2018). https://doi.org/10.1088/1742-6596/979/1/012021.
22. A. Amirjani and D. F. Haghshenas, Sens. Actuat. B Chem. **273**, 1768 (2018). https://doi.org/10.1016/j.snb.2018.07.089.
23. D. Verma, D. Chauhan, M. Das Mukherjee, K. R. Ranjan, A. K. Yadav, and P. R. Solanki, J. Appl. Electrochem. **51**, 447 (2021). https://doi.org/10.1007/s10800-020-01511-3.
24. M. A. Reshchikov, J. Appl. Phys. **129**, 121101 (2021). https://doi.org/10.1063/5.0041608.

25. Y. Yomogida, K. Horiuchi, R. Okada, H. Kawai, Y. Ichinose, H. Nishidome, K. Ueji, N. Komatsu, W. Gao, J. Kono, and K. Yanagi, Sci. Rep. **12**, 101 (2022). https://doi.org/10.1038/s41598-021-03911-7.
26. H.-S. Kim and K.-U. Jang, J. Korean Instit. Elect. Elect. Mat. Eng. **26**, 325 (2013). https://doi.org/10.4313/JKEM.2013.26.4.325.
27. R. Saive, IEEE J. Photovolt. **9**, 1477 (2019). https://doi.org/10.1109/JPHOTOV.2019.2930409.
28. E. Y. Salih, Opt. Mat. **149**, 115120 (2024). https://doi.org/10.1016/j.optmat.2024.115120.
29. Y. Lee, S. H. Yu, J. Jeon, H. Kim, J. Y. Lee, H. Kim, J.-H. Ahn, E. Hwang, and J. H. Cho, Carbon **88**, 165 (2015). https://doi.org/10.1016/j.carbon.2015.02.071.
30. S. H. Yu, Y. Lee, S. K. Jang, J. Kang, J. Jeon, C. Lee, J. Y. Lee, H. Kim, E. Hwang, S. Lee, and J. H. Cho, ACS Nano **8**, 8285 (2014). https://doi.org/10.1021/nn502715h.
31. D. Capista, M. Passacantando, L. Lozzi, E. Faella, F. Giubileo, and A. Di Bartolomeo, Electronics **11**, 271 (2022). https://doi.org/10.3390/electronics11020271.
32. L. Zhuo, P. Fan, S. Zhang, X. Liu, X. Guo, Y. Zhang, Y. Zhan, D. Li, Z. Che, W. Zhu, H. Zheng, J. Tang, J. Zhang, Y. Zhong, Y. Luo, J. Yu, and Z. Chen, Nanoscale **12**, 14188 (2020). https://doi.org/10.1039/D0NR00139B.
33. N. Fu, J. Zhang, Y. He, X. Lv, S. Guo, X. Wang, B. Zhao, G. Chen, and L. Wang, Sensors **23**, 3104 (2023). https://doi.org/10.3390/s23063104.


# كاشف التوصيل الضوئي واسع النطاق المعتمد على انابيب الكربون النانوية المزينة بجسيمات الفضة النانوية


**تقوى يعرب يوسف[1] وشهد عماد حسن[1] وأسامة ناطق ناجي[2] وإستبرق عباس عبد[1]**

*[1] قسم الطاقة المتجددة، كلية علوم الطاقة والبيئة، جامعة الكرخ للعلوم، بغداد، العراق*

*[2] قسم الفيزياء، كلية العلوم، جامعة بغداد، بغداد، العراق*



## الخلاصة

تم توضيح العملية المنهجية لتصنيع الكاشف الضوئي واسع النطاق Ag- MWCNT / SWCNT ،في هذه المقالة، عبر تقنيات الانفجار الكهربائي للسلك، الخلط المباشر للمواد وتقنية الصب النقطي. تم التحقق بدقة من التحليل المجهري لطبوغرافية السطح، البصري، الكهربائي والاستجابة الضوئية للطبقات المصنعة. أظهرت الدراسة الطبوغرافية على وجه التحديد أن قطر الفضة النانوية يتراوح من 85 إلى 82 نانومتر. ومع ذلك، شوهدت ظاهرة امتصاص واسعة في الأطياف الضوئية للطبقات البارزة ضمن المدى (200 إلى800 نانومتر) . كما أظهرت الأجهزة المصنعة من Ag- SWCNT / MWCNT رقما معنويا من مزايا الكاشف كدالة للطول الموجي وقوة الإضاءة (365 و460 و808 نانومتر) استجابة لفرق الجهد المسلط من0 إلى 10 فولت. تم قياس الاستجابية الضوئية للكاشف$R_\lambda$ تحت الطول الموجي للإضاءة (808 نانومتر) 0.575 و0.06 (A / W) ل MWCNTs-Ag وSWCNTs-Ag، على التوالي. كما وجد أن معامل الارتباط لخصائص الأجهزة المصنعة ذو علاقة خطية كدالة للطول الموجي المسلط.



**الكلمات المفتاحية:** كاشف ضوئي، SWCNT، MWCNT، واسع النطاق، الاستجابة الضوئية.